

## Effects of Electrolyte pH on the Electrochemical Behavior of Fe-Based Bulk Metallic Glass

S. L. Wang<sup>1</sup>, H.X. Li<sup>2</sup>, Y. U. Jeong<sup>3</sup>, and S. Yi<sup>4,\*</sup>

<sup>1</sup>School of Aeronautical Manufacturing Engineering, Nanchang Hangkong University, Nanchang, 330063, China

<sup>2</sup>State Key Laboratory for Advanced Metals and Materials, University of Science and Technology Beijing, Beijing, 100083, China

<sup>3</sup>Department of Electronic Materials Science and Engineering, Kyungpook National University, Daegu, 702-701 South Korea

<sup>4</sup>Department of Materials Science and Metallurgy, Kyungpook National University, Daegu, 702-701 South Korea

(received date: 10 August 2011 / accepted date: 19 December 2011)

The effects of electrolyte pH on the electrochemical behavior of Fe-based bulk metallic glass with a composition of  $\text{Fe}_{68.8}\text{C}_{7.0}\text{Si}_{3.5}\text{B}_5\text{P}_{9.6}\text{Cr}_{2.1}\text{Mo}_{2.0}\text{Al}_{2.0}$  were investigated at an ambient temperature. The results indicate that corrosion behavior is strongly dependent on the pH values. The corrosion current densities and capacitance values decrease with an increase in pH values in acidic electrolytes, while the opposite tendencies are obtained in alkaline electrolytes. While the corrosion product of the outer layer in low pH conditions is an amorphous structure, crystalline ferric oxide is obtained in the electrolyte with pH=14. The electrochemical behavior is discussed on the basis of the results of electrochemical and microstructural analysis.

**Key words:** amorphous materials, casting, electrochemistry, SEM, corrosion

### 1. INTRODUCTION

Fe-based bulk metallic glasses (Fe-BMGs) are promising materials for various industrial applications since they have various interesting properties [1-3]. Though their extensive use as bulk structural materials are limited due to the extremely poor tensile ductility of Fe-BMGs, the Fe-BMGs with high glass forming ability (GFA) can be used in practice as anti-wear or anti-corrosive coating materials for metallic components [4,5]. The amorphous coating of Fe-Cr-Mo-C-B-Y [6] was spontaneously passivated with a wide passive region and low passive current density in acid electrolytes. However, active dissolution and no passivation were observed in the polarization curve as the absence of a protective passive film for a Fe-Co-B-Si-Nb bulk metallic glass alloy in a NaCl electrolyte [7]. The Fe-Ni-B glassy alloy [8] was susceptible to pitting in a 3.5% NaCl solution, while it was immune to pitting in a 7N NaOH solution. Due to various environmental conditions, these Fe-based metallic glasses exhibited different corrosion behavior. Therefore, it is inter-

esting to investigate the effect of electrolyte pH on corrosion behavior. In addition to excellent corrosion resistance, the cost-effectiveness for the alloy design and material processing are also important factors for practical applications of Fe-BMGs as coating materials. As a part of developing Fe-BMGs as coating materials that can be produced cost-effectively in large quantities, Fe-BMGs with a high GFA and corrosion resistance have been developed using cast iron and commercial raw materials [9, 10]. In this study, the effects of electrolyte pH on the electrochemical behavior of the Fe-BMG with composition of  $\text{Fe}_{68.8}\text{C}_{7.0}\text{Si}_{3.5}\text{B}_5\text{P}_{9.6}\text{Cr}_{2.1}\text{Mo}_{2.0}\text{Al}_{2.0}$  were systematically investigated in ambient conditions.

### 2. EXPERIMENTAL PROCEDURES

The glassy alloys were fabricated into cylindrical rods by suction of the molten alloys into a water-cooling copper mold in an argon atmosphere, and molten alloys were prepared with industrial raw materials using an arc-melting process in an argon atmosphere. The chemical compositions of the raw materials were listed in the literature [11]. The structure of the specimens for the corrosion test was analyzed by X-ray diffraction (XRD, Philip X'Pert diffractometer) with

\*Corresponding author: yish@knu.ac.kr

©KIM and Springer, Published 10 October 2012

Cu radiation ( $\text{Cu-K}\alpha$ ,  $\lambda=0.1541 \text{ nm}$ ). XRD results showed that all of the specimens used in corrosion measurement were amorphous. The electrolytes with pH=0 and pH=2 were prepared with  $\text{H}_2\text{SO}_4$  acid of 98 wt%. The electrolytes with pH=12 and pH=14 were prepared with NaOH. The electrolytes with various pH levels (pH=4–10) were prepared through the addition of NaOH in the 0.01 M  $\text{H}_2\text{SO}_4$  electrolyte.

Electrochemical measurements were conducted by a potentiostat (EG&G Princeton Applied Research PARSTAT 2273 with EG&G powersuit software) and a three-electrode cell. The counter electrode was graphite and the reference electrode was a saturated calomel electrode (SCE). The potentiodynamic polarization curves were measured with a scan rate of 50 mV/min and the potentiostatic polarization curves were conducted by applying a potential of 0.45 V vs. SCE for 30 min. The electrochemical impedance was measured from 50 mHz to 50 kHz with the AC mode after the specimens were immersed for 20 min to obtain a stable open circuit potential. The amplitude of the AC signal applied between both electrodes was 10 mV. After immersion for 15 days, the surface morphologies were observed by scanning electron microscope (SEM, HITACHI 4300). The chemical characterization on the surface after potentiostatic polarization for 30 min was analyzed by X-ray photoelectron spectroscopy (XPS, Quantera SXM photoelectron spectroscopy). The XPS data were collected using monochromatized Al-K $\alpha$  radiation at 1486.92 eV.

### 3. RESULTS AND DISCUSSION

The potentiodynamic polarization curves of a  $\text{Fe}_{68.8}\text{C}_{7.0}\text{Si}_{3.5}\text{B}_5\text{P}_{9.6}\text{Cr}_{2.1}\text{Mo}_{2.0}\text{Al}_{2.0}$  amorphous alloy in the electrolytes with various pH values are plotted in Fig. 1, and the corrosion potentials ( $E_{\text{Corr}}$ ) and corrosion current densities ( $I_{\text{Corr}}$ ) in

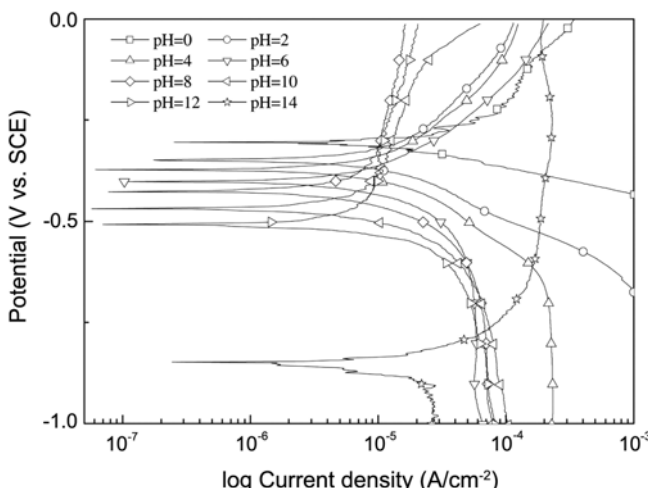


**Fig. 1.** Potentiodynamic polarization in the electrolytes with various pH values.

**Table 1.** Results of potentiodynamic polarization and impedance in the electrolytes with various pH

pH	$E_{\text{corr}}$ (-mV)	$I_{\text{corr}}$ ( $\mu\text{A}/\text{cm}^2$ )	$R_{ct}$ ( $\Omega\text{cm}^2$ )	$C_{dl}$ ( $\text{F}/\text{cm}^2$ )	$\phi$
0	305.1	51.2	1067	$6.25 \times 10^{-4}$	9.1
2	349.0	30.1	4471	$9.57 \times 10^{-5}$	9.4
4	371.9	21.5	12510	$7.75 \times 10^{-5}$	9.9
6	401.2	17.9	27920	$3.66 \times 10^{-5}$	8.2
8	425.5	13.4	63780	$3.26 \times 10^{-5}$	11.0
10	468.3	15.8	41730	$4.57 \times 10^{-5}$	10.4
12	506.1	17.1	28360	$6.57 \times 10^{-5}$	9.5
14	851.3	31.5	2314	$4.33 \times 10^{-4}$	26.2

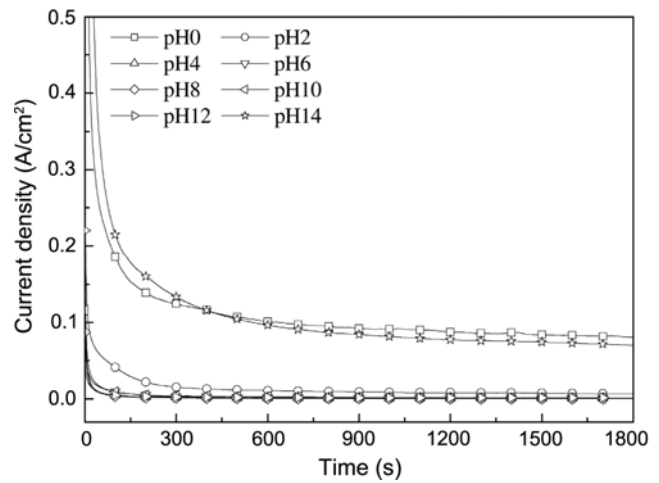


**Fig. 2.** Potentiostatic polarization in the electrolytes with various pH values.

the electrolytes with various pH values are summarized in Table 1. The corrosion potentials ( $E_{\text{Corr}}$ ) decreased with an increase in pH values, while the corrosion current densities ( $I_{\text{Corr}}$ ) decreased, reached a minimum value in the neutral electrolyte, and then increased. The tendency of corrosion current densities may depend on the ion concentrations in the electrolytes. Higher corrosion current densities were obtained in the electrolytes with higher concentrations of  $\text{H}^+$  or  $\text{OH}^-$  ions [12].

The observed current density vs. passivation time during the potentiostatic polarization in the electrolytes of various pH values is shown in Fig. 2. The applied potential of 0.45 V vs. SCE was selected from the potentiodynamic polarization curves. The current densities decreased continuously with time and finally reach a steady state current density ( $I_{ss}$ ). Such smooth shapes of the curves indicate that a stable layer formed on the surface during the entire measurement period.

Electrochemical impedance spectroscopy (EIS) measurements were performed in order to investigate the kinetic stability of the surface oxide layer in the electrolytes of various pH values. The Nyquist plots of  $\text{Fe}_{68.8}\text{C}_{7.0}\text{Si}_{3.5}\text{B}_5\text{P}_{9.6}\text{Cr}_{2.1}\text{Mo}_{2.0}\text{Al}_{2.0}$  glass are shown in Fig. 3. The experimental data in the figure are presented as symbols and the solid lines were obtained

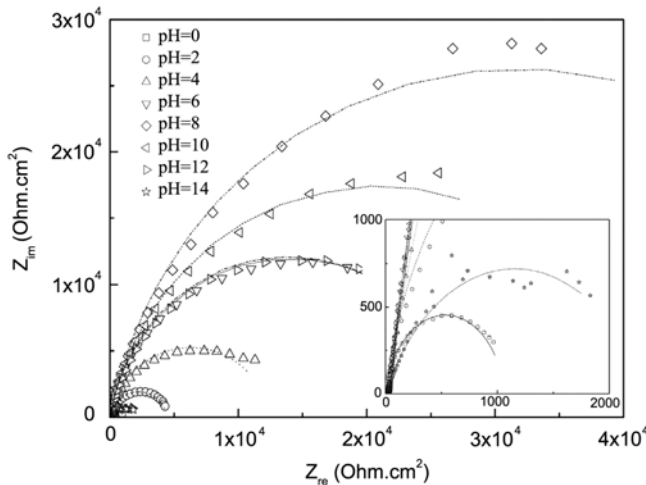


Fig. 3. Nyquist plot of the electrolytes with various pH values.

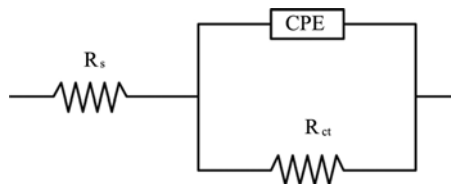


Fig. 4. Equivalent circuit for the fitting of impedance results.

by curve fitting using non-linear-least-square fit analysis. The equivalent circuit is illustrated in Fig. 4.  $R_s$  and  $R_{ct}$  are the electrolyte and charge transfer resistance, respectively; CPE is the constant phase element related to the double layer capacitance of the electrode ( $C_{dl}$ ). The impedance of the constant phase element was described in [13,14]:

$$Z_{CPE} = [C(j\omega)^{(1-\alpha)}]^{-1} \quad (1)$$

where  $\omega$  is the angular frequency of the AC voltage,  $j = \sqrt{-1}$ ,  $\alpha$  is the frequency independent parameter related to the depression angle  $\varphi$  which is equal to  $\alpha \times 90^\circ$ , and  $C$  is a constant related to the double layer capacitance of the electrodes ( $C_{dl}$ ) by the following equation:

$$C = C_{dl}^{(1-\alpha)}(R_s^{-1} + R_{ct}^{-1})^\alpha \quad (2)$$

when  $\alpha = 0$ ,  $C$  corresponds to  $C_{dl}$ ; when  $\alpha = 1$ ,  $C$  is a resistance; when  $\alpha = -1$ ,  $C$  is an inductance.

The parameters obtained by the fitting procedure of EIS experimental data of the investigated electrodes are also listed in Table 1. The charge transfer resistance ( $R_{ct}$ ) increased initially with the pH, reached a maximum value in the neutral electrolytes, and then decreased with the pH of the electrolyte. The opposite behavior was observed for the pH dependence of the capacitance ( $C_{dl}$ ) and corrosion current density ( $I_{Corr}$ ). In electrolytes with higher hydrogen ions or hydroxyl

ions, the corrosion processes were faster; higher  $I_{Corr}$  and  $C_{dl}$  were obtained due to the rough surface on the electrodes [15]. The increase of the charge transfer resistance ( $R_{ct}$ ) indicates an increase in the insulating character of the oxide films [16]. The thickness of the passive films ( $L_{ss}$ ) on the interface/electrolyte can be estimated from the capacitance data using the well-known ‘parallel plate’ expression [17]:

$$L_{ss} = \frac{\epsilon_0 \epsilon}{C_{dl}} A \quad (3)$$

where  $\epsilon$  is the dielectric constant of the porous layer,  $\epsilon_0$  is the vacuum permittivity, and  $A$  is the surface area of the electrode. Therefore, it can be inferred from equation (3) that the thickness of the passive film formed in weak acidic and alkaline electrolytes is thicker than that formed in strong acidic and alkaline electrolytes.

The microstructures of the specimens were analyzed by scanning electron microscopy, as shown in Fig. 5 and Fig. 6. A ‘dried riverbed’ cracked structure formed on the surface of the specimen immersed in the electrolytes of pH=0 and pH=2, as shown in Figs. 5(a) and (b). While many small cracks were found on the surface with a value of pH=4, no cracks were observed on the surface of the specimen immersed in the electrolyte with a value of pH=6. In the high pH electrolytes, smooth surfaces without cracks were obtained for all specimens, and are shown in Fig. 6. The microstructure with an acicular shape was observed in a high magnification image, which is shown in Fig. 6(d). These results indicate the surface roughness also depends on the pH value of the electrolytes, and might provide evidence for the tendency of a double layer capacitance ( $C_{dl}$ ) in electrolytes with various pH values.

Due to the similarity of surface morphologies in acidic electrolytes and alkaline electrolytes, an energy dispersive

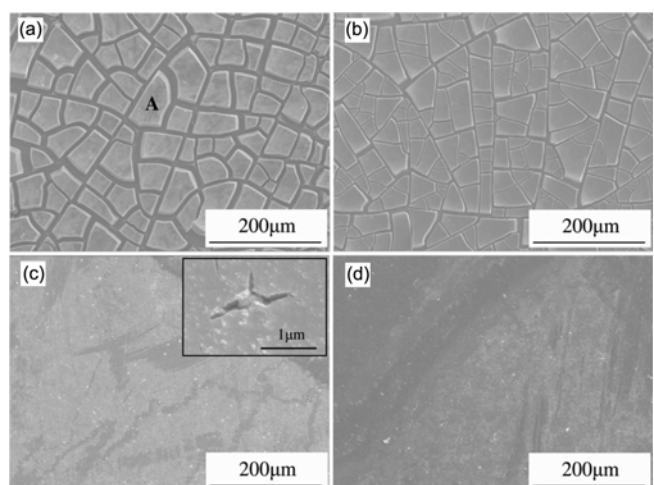
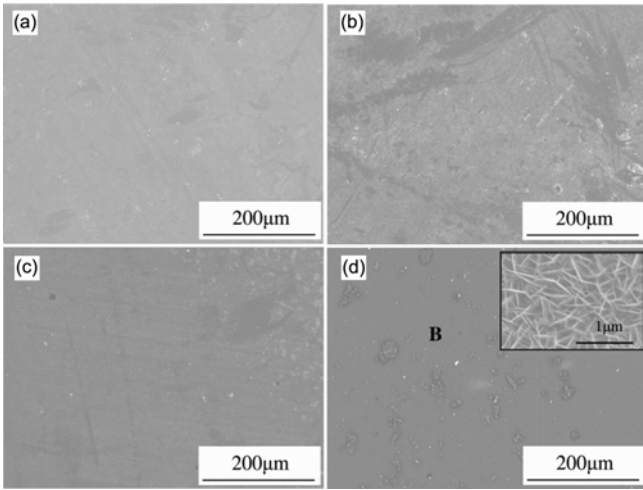
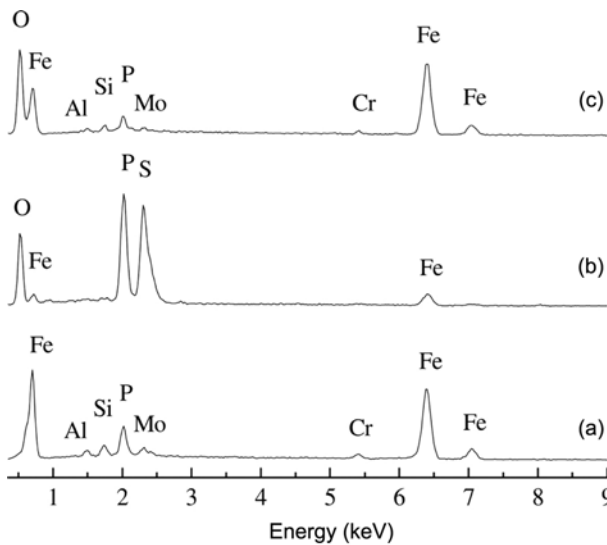


Fig. 5. Surface morphologies of the specimens immersed in acidic electrolytes: (a) pH=0, (b) pH=2, (c) pH=4, and (d) pH=6.



**Fig. 6.** Surface morphologies of the specimens immersed in alkaline electrolytes: (a) pH=8, (b) pH=10, (c) pH=12, and (d) pH=14.



**Fig. 7.** Results of EDS for the specimens with the conditions of as-cast (a), pH=0 (b), and pH=14 (c).

spectroscopy (EDS) analysis was performed on the selected area, ‘A’ and ‘B’, of the specimen immersed in the electrolytes with pH=0 and pH=14, respectively. As shown in Fig. 7, two specimens were compared with the as-cast specimen. The corrosion product near the cracks was composed of iron, phosphorus, sulfur, and oxygen, and the corrosion product with acicular microstructure was oxygen-rich. In order to identify the phases of the corrosion product, X-ray diffraction was carried out for specimens with various pH conditions, and is shown in Fig. 8. Crystalline peaks were not observed for the specimens immersed in the electrolytes of various pH values from 0 to 12, while the crystalline peak of a  $\text{Fe}_2\text{O}_3$  phase was detected for the specimen with an electrolyte of pH=14. A similar result was reported in which a

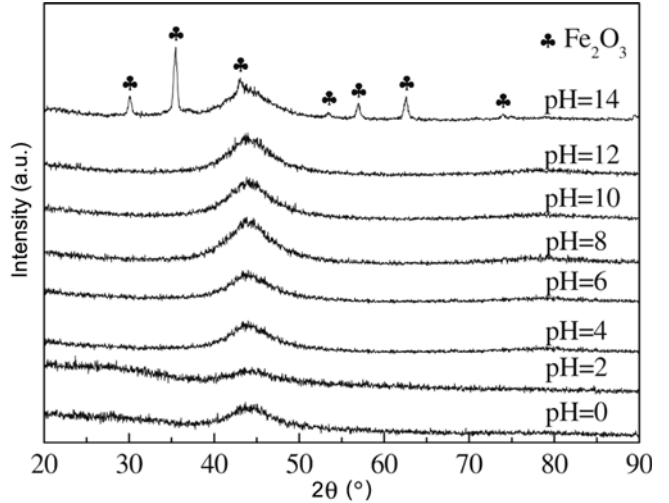


**Fig. 8.** XRD patterns of the specimens with various pH conditions.

$\text{Fe}_2\text{O}_3$  phase was observed on the surface of stainless steel after the cyclic voltammetry in a NaOH electrolyte [18].

The passive films on the specimens after potentiostatic polarization with various pH conditions were analyzed by X-ray photoelectron spectroscopy (XPS). The main information about the film composition was obtained from XPS analysis as shown in Fig. 9 and Fig. 10. The photo-electron signals and curve fitting of the specimens in the electrolyte with pH=0 are shown in Fig. 9. Figure 9(a) reveals that Cr 2p<sub>3/2</sub> spectrum contains three components: chromium (III) oxide  $\text{Cr}_2\text{O}_3$ , chromium (III) hydroxide  $\text{Cr}(\text{OH})_3$  and chromic salt  $\text{Cr}_2(\text{SO}_4)_3$ . Fe 2p<sub>3/2</sub> signals were composed of four components: iron (II) oxide  $\text{FeO}$ , iron (III) oxide  $\text{Fe}_2\text{O}_3$ , iron (III) oxy-hydroxide  $\text{FeOOH}$  and ferrous salt  $\text{FeSO}_4$ , which is shown in Fig. 9(b). Figure 9(c) shows a Mo 3d<sub>5/2</sub> spectrum containing molybdenum (VI) oxide  $\text{MoO}_3$ . Three contributions are detected in O 1s spectra as shown in Fig. 9(d): the first part assigned to oxygen in metal oxides, the second part to metal hydroxide groups, the third part to adsorbed water. In the case of pH=14, no  $\text{Cr}^{3+}$  salt or  $\text{Fe}^{2+}$  salt were observed, which is shown in Fig. 10. The binding energy  $E_b$  with  $\pm 0.3$  eV fluctuation for the components of the passive film is listed in Table 2. These results agree with the data published in the literature [19-23].

It is generally agreed that the components of passive film affecting the protective quality are usually determined by the composition of the alloy system and the ambient environment. The chromium was the effective element for passivation in Fe-based BMG [24] and the formation of chromium-rich passive film was responsible for the high corrosion resistance [25]. A passive film composed of a double layer, an outer layer of iron-rich oxides and an inner layer of chromium-rich oxides was reported in the literature [26]. When some iron was substituted with Ta in a Fe-Cr-Ni-Ta alloy, the passive film was significantly richer in tantalum and chro-

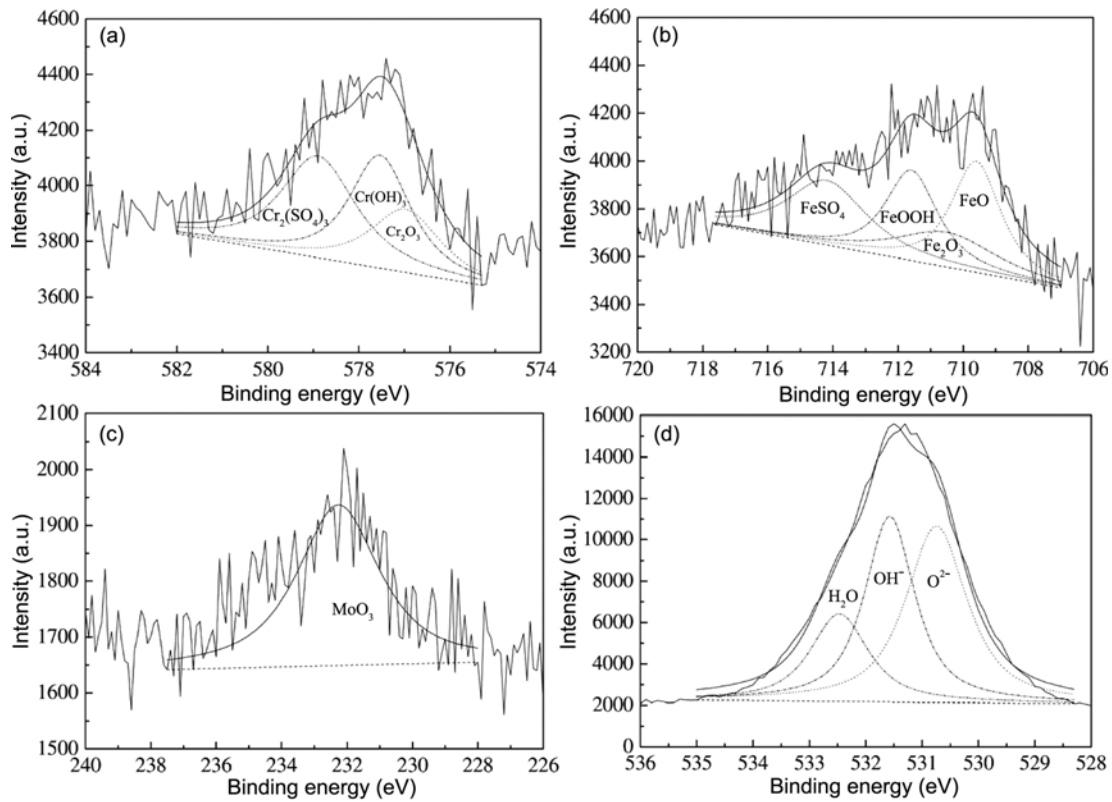


**Fig. 9.** Results of XPS of the specimens immersed in the electrolyte with pH=0. (a) Cr 2p<sub>3/2</sub>, (b) Fe 2p<sub>3/2</sub>, (c) Mo 3d<sub>5/2</sub>, and (d) O 1s

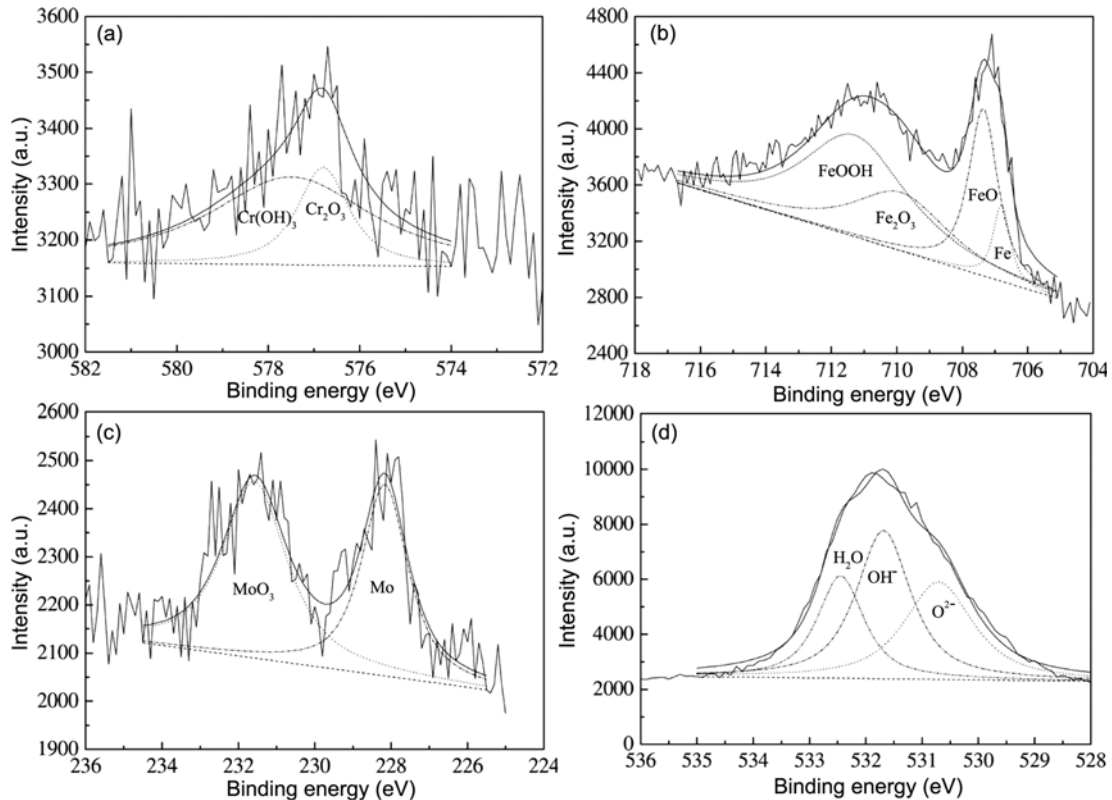


**Fig. 10.** Results of XPS of the specimens immersed in the electrolyte with pH=14. (a) Cr 2p<sub>3/2</sub>, (b) Fe 2p<sub>3/2</sub>, (c) Mo 3d<sub>5/2</sub>, and (d) O 1s

**Table 2.** XPS peak positions for the components of corrosion products

Spectra	Components	pH=0	pH=14
Cr2p <sub>3/2</sub>	Cr <sub>2</sub> O <sub>3</sub>	576.9	576.8
	Cr(OH) <sub>3</sub>	577.5	577.5
	Cr <sub>2</sub> (SO <sub>4</sub> ) <sub>3</sub>	578.9	--
Fe2p <sub>3/2</sub>	Fe	--	706.8
	FeO	709.6	707.4
	Fe <sub>2</sub> O <sub>3</sub>	710.5	709.9
Mo3d <sub>5/2</sub>	FeOOH	711.6	711.3
	FeSO <sub>4</sub>	714.2	--
	Mo	--	228.2
O1s	MoO <sub>3</sub>	232.3	231.6
	O <sup>2-</sup>	530.7	530.7
	OH <sup>-</sup>	531.6	531.7
O1s	H <sub>2</sub> O	532.5	532.5

mium ions, and greatly deficient in iron ions [27]. The authors of [28,29] reported that the passive film consisted of iron-chromium-molybdenum oxyhydroxide with air exposure, while the formation of molybdenum oxyhydroxide, not chromium-rich oxyhydroxide, was responsible for the improvement of corrosion resistance for a Fe-Cr-Mo-P-C alloy immersed in deaerated 1 M HCl. In this study, the passive film was composed of ferric, chromic and molybdenum oxides in various pH electrolytes.

The amorphous structures for the corrosion products in the electrolytes of various pH values (pH=0-6) may be inferred from the XRD result since only a broad peak was detected. The amorphous structure of corrosion products on stainless steel was reported in a sulfuric electrolyte [30]. Since iron is not stable and dissolves and metalloid elements such as B and P [31-33] are hydrolyzed easily in an acid electrolyte, the ions of Fe<sup>2+</sup>, H<sub>2</sub>PO<sub>4</sub><sup>-</sup> and H<sub>2</sub>BO<sub>3</sub><sup>-</sup> forms in the acid electrolyte. As the reactions proceed, the occurrence of supersaturated FeSO<sub>4</sub> and Fe(H<sub>2</sub>PO<sub>4</sub>)<sub>2</sub> is possible in the vicinity of the electrode surface as the migration of Fe<sup>2+</sup> ions is not quick enough. Therefore, some ferrous sulphate, phospholite salts [33,34] are precipitated and adsorbed on the electrode surface.

In an alkaline electrolyte, it is well known that Fe<sub>2</sub>O<sub>3</sub> is stable. During passivation, the outward dissolution of Fe ion is faster than that of other metal ions [26], so a greater amount of Fe<sub>2</sub>O<sub>3</sub> is precipitated to the outermost surface, and this was identified by SEM and XRD. However, crystalline peaks were not detected on the specimen surfaces immersed in the electrolytes with pH=8, pH=10 and pH=12, and this might be due to the low fraction of the crystalline phases which could not be detected by XRD.

#### 4. CONCLUSIONS

The effects of electrolyte pH on the electrochemical behavior of Fe-based bulk metallic glass with a composition

of Fe<sub>68.8</sub>C<sub>7.0</sub>Si<sub>3.5</sub>B<sub>5</sub>P<sub>9.6</sub>Cr<sub>2.1</sub>Mo<sub>2.0</sub>Al<sub>2.0</sub> were investigated in an ambient temperature. The results indicate that corrosion behavior is strongly dependent on the pH of electrolytes.

(1) Corrosion potential (E<sub>corr</sub>) decreases with an increase in the pH value, while the corrosion current density (I<sub>corr</sub>) decreases, reaches a minimum value in the neutral electrolyte, and then increases.

(2) While the charge transfer resistance (R<sub>ct</sub>) increases up to the neutral pH value and then decreases with the pH of the electrolyte, the corrosion current density (I<sub>corr</sub>) and the capacitance (C<sub>dl</sub>) exhibit similar behavior of pH dependence.

(3) The components on the metal/film interface were analyzed by XPS, and the oxides and hydroxides of iron and chromium were found in both acidic and alkaline electrolytes. In the electrolyte with a low pH, the corrosion products in the outer layer had an amorphous structure, but ferric oxide was observed on the outer layer of the specimen immersed in the electrolyte of pH=14.

#### ACKNOWLEDGMENTS

The work was supported by the National Natural Science Foundation of China (Grants No.51165038), the Doctoral Startup Fund of Nanchang Hangkong University (EA201103238), the Korean Ministry of Commerce, Industry and Energy through the project entitled as “The development of structural metallic materials and parts with super strength and high performance”.

#### REFERENCES

1. A. L. Greer, *Science* **267**, 1947 (1995).
2. K. Pekala, J. Latuch, and T. Kulik, *Mater. Sci. Eng. A* **375**, 377 (2004).
3. A. Inoue, B. L. Shen, and C. T. Chang, *Intermetallics* **14**, 936 (2006).
4. A. Basu, A. N. Samant, S. P. Harimkar, *Surf. Coat. Tech.* **202**, 2623 (2008).
5. I. Manna, J. D. Majumdar, B. R. Chandra, *Surf. Coat. Tech.* **201**, 434 (2006).
6. Z. Zhou, L. Wang, and F. C. Wang, *Surf. Coat. Tech.* **204**, 563 (2009).
7. Z. L. Long, Y. Shao, and A. Inoue, *Intermetallics* **15**, 1453 (2007).
8. A. Lekatou, A. Marinou, P. Pasalas, *J. Alloys Compd.* **483**, 514 (2009).
9. H. X. Li, Z. P. Lu, and S. Yi, *Met. Mater. Int.* **15**, 7 (2009).
10. H. X. Li and S. Yi, *Mater. Chem. Phys.* **112**, 305 (2008).
11. S. L. Wang, H. X. Li, and S. Yi, *Mater. Chem. Phys.* **113**, 878 (2009).
12. S. Hiromoto, A. P. Tsai, and M. Sumita, *Corros. Sci.* **42**, 2193 (2000).
13. C. P. Lee, C. C. Chang, and H. C. Shih, *Corros. Sci.* **50**,

- 2053 (2008).
- 14. M. P. M. Kaninski and V. M. Nikolic, *Int. J. Hydrogen Energ.* **34**, 703 (2009).
  - 15. H. O. Cirkovic, E.S. Lisac, and H. Takenouti, *Corros. Sci.* **52**, 398 (2010).
  - 16. F. Rosalbino, S. Delsante, and G. Borzone, *Corros. Sci.* **52**, 322 (2010).
  - 17. J. Liu and D. D. Madonald, *J. Electrochem. Soc.* **148**, 425 (2001).
  - 18. C. M. Abreu, M. J. Cristobal, and R. Losada, *Electrochim. Acta* **51**, 2991 (2006).
  - 19. G. E. Muilenberg and C. D. Wagner, *Handbook of X-Ray Photoelectron Spectroscopy*, Perkin-Elmer, USA (1979).
  - 20. M. L. Varsanyi, F. Falkenberg, and I. Olefjord, *Electrochim. Acta* **43**, 187 (1998).
  - 21. H. Alves, M. G. S. Ferrira, and U. Koster, *Corros. Sci.* **45**, 1833 (2003).
  - 22. P. Keller and H. H. Strehblow, *Corros. Sci.* **46**, 1939 (2004).
  - 23. A. A. Hermas, *Corros. Sci.* **50**, 2498 (2008).
  - 24. A. Pardo, M. C. Merino, and E. Otero, *J. Non-Cryst. Solids* **352**, 3179 (2006).
  - 25. S. J. Pang, T. Zhang, and A. Inoue, *Corros. Sci.* **44**, 1847 (2002).
  - 26. C. T. Liu and J. K. Wu, *Corros. Sci.* **49**, 2189 (2007).
  - 27. X. Y. Li, E. Akiyama, and K. Hashimoto, *Corros. Sci.* **41**, 1849 (1999).
  - 28. M. W. Tan, E. Akiyama, and A. Kawashima, *Corros. Sci.* **37**, 331 (1995).
  - 29. M. W. Tan, E. Akiyama, and A. Kawashima, *Corros. Sci.* **38**, 349 (1996).
  - 30. M. Nakatsu, S. Yonezawa, and M. Taashima, *Corros. Sci.* **49**, 3185 (2007).
  - 31. T. P. Moffat and W. F. Flanagan, *J. Electrochem. Soc.* **135**, 2712 (1988).
  - 32. I. Chattoraj, K. R. M. Rao, and A. Mitra, *Corros. Sci.* **41**, 1 (1999).
  - 33. S. Virtanen and H. Boehni, *ISIJ International* **31**, 229 (1991).
  - 34. G. L. Song, C. N. Cao, and S. H. Chen, *Corros. Sci.* **47**, 323 (2005).